
# Polydopamine Modified Carbon Nitride and PAMAM Assembled Electrochemical Immunosensor for Detection of Indole-3-Acetic Acid

ChemElectroChem

Research Article
doi.org/10.1002/celc.202400145

Chemistry Europe
European Chemical Societies Publishing

www.chemelectrochem.org

# Polydopamine Modified Carbon Nitride and PAMAM Assembled Electrochemical Immunosensor for Detection of Indole-3-Acetic Acid

Jian Zhang,[a] Aixue Li,[b] Xin Yu,[c] Ivan Mijakovic,[a, d] and Santosh Pandit*[a]

Indole-3-acetic acid (IAA) assumes a pivotal role as a phytohormone of utmost importance, intricately orchestrating the nuanced processes associated with the growth and developmental trajectories of botanical organisms. In this study, we have designed and fabricated a label-free electrochemical impedance immunosensor for the precise detection of IAA. The detection strategy predominantly relied upon polydopamine modified carbon nitride ($C_3N_4$) nanosheets (PCN) and polyamidoamine (PAMAM) dendrimer. Through the modification with PCN and PAMAM, the electrode has increased the active area and enhanced the immobilization capacity of antibodies for IAA. The immunosensor's ability to capture IAA was significantly improved by enhancing the immunoreaction between the antibody and antigen. This enhancement led to an increased response in the electrochemical behavior of the $Fe(CN)_6^{3-/4-}$ redox probe. The impedance immunosensor developed exhibits remarkable sensitivity, exceptional selectivity, and consistent performance in the detection of IAA. This assay method, with the potential to replace antibodies, could offer an alternative approach for detecting various phytohormones.

## 1. Introduction

Indole-3-acetic acid (IAA) functions as a natural plant hormone pivotal for governing plant growth. Its extensive application in agricultural production underscores its significance in fostering robust crop development.[1] IAA is present in all organs of the plants and is mainly concentrated in areas of vigorous growth such as the tips of growing shoots and roots, unfolding leaves, embryos and seeds.[2] IAA is considered a regulator for some important biological processes for plants, including cell elongation, division, differentiation, and organogenesis.[3] Precise quantification of IAA in plants is critical for enhanced regulation of plant growth and development and development of sustainable agriculture. Quantitative analysis of IAA can be done using various methods, such as high-performance liquid chromatography,[4] gas chromatography-mass spectrometry,[5] capillary electrophoresis,[6] and enzyme linked immunosorbent assay.[7] Nevertheless, these methods are typically costly and time-intensive. Various electrochemical detection methods have been developed to detect IAA such as differential pulse voltammetry (DPV), square wave voltammetry (SWV), electrochemical impedance spectroscopy (EIS) and linear sweep voltammetry (LSV).[8–11] Electrochemical sensors IAA offer several advantages over traditional detection methods, such as higher sensitivity, minimal detection threshold and rapid response time.[12–14] The interaction between IAA and sensor can be facilitated by immobilizing a biological recognition element such as enzyme or antibody on the electrode surface, which specifically binds to IAA and induces a change in the electrochemical signal. Nanomaterials, including graphene, carbon nanotubes, metal nanoparticles, and metal-organic frameworks, have been utilized in electrochemical sensors to improve their sensitivity and selectivity for detection of IAA.[15–18] Nanomaterial-modified electrochemical sensors benefit from the fact that nanomaterials can enhance the electron transfer between IAA molecules and the electrode surface. In addition, the high surface area of nanomaterials can improve the assembly of biorecognition elements on the electrode surface.[19]

Carbon nitride ($C_3N_4$) has attracted attention for its potential applications in fields such as photocatalysis, energy storage, and electronic devices.[20,21] $C_3N_4$ is a two-dimensional material composed of carbon and nitrogen atoms arranged in a hexagonal lattice structure. $C_3N_4$ has a high surface area, excellent thermal and chemical stability, and can be synthesized using low-cost precursors. $C_3N_4$ have been investigated as a potential biosensing material for diagnosis and detection applications.[22] $C_3N_4$ possesses the capacity to enhance the anchoring and electron transference of biomolecules, such as enzymes or antibodies, onto the electrode surface. This augmentation contributes to an elevation in both the specificity

[a] J. Zhang, I. Mijakovic, S. Pandit
Systems and Synthetic Biology Division, Department of Life Sciences, Chalmers University of Technology, SE-412 96 Gothenburg, Sweden
E-mail: pandit@chalmers.se

[b] A. Li
Research Center of Intelligent Equipment, Beijing Academy of Agriculture and Forestry Sciences, Beijing 100097, China

[c] X. Yu
Institute for Advanced Interdisciplinary Research, School of Chemistry and Chemical Engineering, University of Jinan, Jinan 250022, China

[d] I. Mijakovic
The Novo Nordisk Foundation, Center for Biosustainability, Technical University of Denmark, DK-2800 Kogens Lyngby, Denmark

Supporting information for this article is available on the WWW under https://doi.org/10.1002/celc.202400145

and sensitivity of electrochemical biosensors. Furthermore, the distinctive semiconducting characteristics inherent to $C_3N_4$ render it a fitting contender for the realm of photoelectrochemical biosensors.[23] When $C_3N_4$ modified electrode surface recognizes and binds to the target analyte, electron transfer occurs between the molecules and the photoexcited $C_3N_4$, leading to a change in photocurrent, thereby allowing for the quantitative analysis of the substance. However, the use of $C_3N_4$ to construct electrochemical biosensors for the detection of IAA and other plant hormones is rare.

Polydopamine (PDA) is a versatile material formed through the oxidation and polymerization of dopamine. It has the ability to spontaneously deposit onto various objects through self-polymerization, making it a useful material for functional coating applications.[24] Due to its biocompatibility, nontoxicity, and catalytic activity, PDA has been extensively developed in the biosensor fields.[25,26] PDA can be efficiently combined with free amino group-containing molecules using Michael addition and/or Schiff base reactions to introduce specific chemical functionalities or properties.[27] Polyamidoamine (PAMAM) dendrimers have gained significant attention as electrode materials in the development of electrochemical biosensors due to their unique properties.[28,29] PAMAM dendrimers with large number of primary amino groups are highly branched that provides a large surface area for the immobilization of biomolecules, increasing the loading capacity and stability of the biosensor.

In this study, we developed an electrochemical impedance immunosensor for the detection of IAA. The immunosensor was fabricated using a multilayer assembly strategy on Au electrode. The electrode surface was modified with PDA modified $C_3N_4$ nanosheets (PCN), PAMAM, and anti-IAA to achieve selective detection of IAA. The immobilization of PAMAM is achieved by the covalent bonding of the amino group of the dendrimer to PCN through Schiff base and/or Michael addition reactions. PCN and PAMAM modified gold electrode greatly increased the amount of immobilized anti-IAA, enhancing the sensitivity of the immunosensor. The specific binding of IAA to the corresponding antibody blocked the permeation of the redox probe, and the change in electrochemical impedance was used to monitor the immune response. The electrochemical sensor demonstrates exceptional sensitivity, remarkable selectivity, and robust reliability for detecting IAA.

## Experimental Section

### Materials

Dopamine hydrochloride, urea, indole acetic acid (IAA), salicylic acid, ascorbic acid, succinic acid, citric acid, and abscisic acid were sourced from Sigma-Aldrich (St. Louis, MO, US). The G4 ethylenediamine core poly(amidoamine) (PAMAM) dendrimer, monoclonal antibody against IAA, and glutaraldehyde were acquired from Sigma-Aldrich (Germany). All reagents used were of analytical reagent grade.

### Preparation of Polydopamine Modified $C_3N_4$ Nanosheet (PCN)

Bulk $C_3N_4$ synthesis was achieved by subjecting 10 g of urea to thermal polymerization within an alumina crucible. This process was carried out in a muffle furnace with a covered setup, gradually raising the temperature from room temperature to 550 °C at a rate of 1 °C per minute, all under ambient atmospheric conditions. The temperature was maintained at 550 °C for a duration of 2 h. The resulting yellow bulk $C_3N_4$ product was allowed to naturally cool to room temperature. For the generation of $C_3N_4$ nanosheets, the uniform dispersion of bulk $C_3N_4$ within an alumina crucible ensured optimal exposure to the ambient atmosphere. The specimens underwent heat treatment at 550 °C for 3 h with a heating rate of 2 °C/min. This thermal process facilitated the gradual exfoliation of bulk $C_3N_4$ powder, resulting in the formation of $C_3N_4$ nanosheets (CN). Afterward, the samples were harvested, dispersed in ultrapure water, and subjected to consecutive ultrasonication for a duration of 8 hours. Subsequent to this, the specimens underwent a filtration process, were thoroughly washed, and subsequently dried at 80 °C for a period of 6 hours.

Polydopamine modified $C_3N_4$ nanosheet (PCN) was obtained by adding dopamine hydrochloride to an aqueous dispersion of $C_3N_4$ nanosheets. In detail, 200 mg of CN was added to a 400 mL solution of 10 mM Tris-HCl (pH 8.5). The suspension experienced successive ultrasonication for a duration of 30 minutes. Subsequently, 100 mg of dopamine hydrochloride was incorporated into the mixture and stirred for a span of 12 hours. The solution color evolved from a faint yellow hue to a profound black. The resulting black sample was collected, subjected to a washing procedure, and subsequently dialyzed in water over a duration of 3 days to eliminate any surplus dopamine. PCN were separated by filtration and subsequently dried at a temperature of 80 °C for 6 h.

### Characterization

The morphologies of the samples were determined with field-emission scanning electron microscope (SEM, Hitachi S-8100). X-ray photoelectron spectroscopy (XPS) was performed on a PHI 5000 VersaProbe spectrometer. Monochromatized Al Kα (1486.6 eV) X-ray was used to collect the spectra. Spectra were performed using CasaXPS software. X-ray powder diffraction (XRD) data was acquired utilizing an X-ray diffraction spectrometer (D8-advance, Bruker AXS, Germany). Fourier transform infrared spectrum (FTIR) data was acquired with an IR spectrometer (NEXUS 670, America) spanning the range from 4000 to 500 $cm^{-1}$.

### Preparation of the Anti-IAA/PAMAM/PCN/Au Immunosensor

Au electrode, measuring 2 mm in diameter, underwent a meticulous polishing procedure utilizing alumina powder with sizes of 0.3 and 0.05 μm. Following this, the electrode underwent ultrasonic cleaning in deionized water and ethanol before being dried using a stream of nitrogen. Then the Au electrode was rinsed with deionized water and absolute ethanol in sequential steps. Subsequently, 5 μL of aqueous suspension of PCN (0.5 mg/mL) was dropped coating on the surface of this polished and clean Au electrode. Then the PCN modified Au electrode (PCN/Au) was immersed into 5 mg/mL PAMAM solution of 10 mM Tris-HCl (pH 8.5) at 50 °C for 24 h, followed by rinsing with buffer and deionized water to remove excess PAMAM dendrimers for further crosslinking treatment. The PAMAM and PCN-modified Au electrode (PAMAM/PCN/Au) was immersed in a 5% GA solution for 2 h. Following this, 5 μL of the anti-IAA solution (1 mg/mL) was carefully applied to the electrode surface and incubated for 2 h at 4 °C. To minimize nonspecific binding effects, the modified electrode was

subjected to a 30-minute treatment with 1% BSA. The anti-IAA/PAMAM/PCN/Au electrode was rinsed with 10 mM PBS solution (pH 7.4) and stored at 4 °C. The preparation process of the sensor is illustrated in Figure 1.

### Electrochemical Measurements

Electrochemical measurements were conducted utilizing an electrochemical workstation (Gamry Reference 3000, America) that was equipped with a standard three-electrode system. The reference electrode employed was Ag/AgCl (saturated KCl), and a Pt plate with a 1 cm×1 cm surface area served as the counter electrode. The working electrode used was the previously prepared modified Au electrode. The electrochemical measurements were conducted in a 0.01 M PBS with a pH of 7.4, incorporating a 5 mM $Fe(CN)_6^{3-/4-}$ redox probe. Impedance spectra were recorded over a frequency range spanning from 100 mHz to 100 kHz, using a voltage amplitude of 5 mV. For the detection of IAA, a 5 μL solution containing either IAA standard or sample was meticulously administered onto the modified electrode surface and allowed to incubate for one hour in a humid environment. Following incubation, the electrode underwent thorough rinsing with PBS. Following this, impedance spectra were recorded, and the variation in the $R_{ct}$ value ($\Delta R_{ct}$) was employed to determine the IAA concentration.

## 2. Results and Discussions

The X-ray diffraction (XRD) patterns of CN and PCN are shown in Figure 2a. The diffraction peak identified at 27.4° for CN arises from the stacking of layers along the (002) plane of graphitic $C_3N_4$ (JCPDS 87-1526). After modification by PDA, the XRD pattern of PCN is similar with CN, indicating that the presence of PDA does not change the crystalline phase of $C_3N_4$.[30] The Fourier transform infrared spectroscopy (FTIR) spectra of the CN and PCN were tested, as shown in **Fig. 2b**. The CN spectrum displays peaks ranging from 1200 to 1650 $cm^{-1}$, which correspond to the characteristic stretching modes of aromatic CN heterocycles. Additionally, the peak at 810 $cm^{-1}$ is attributed to the out-of-plane bending mode of the triazine unit. The broad peaks observed between 2900 and 3500 $cm^{-1}$ can be attributed to the N–H stretching vibrations caused by uncondensed amino functional groups. PCN spectrum was similar to that of CN, which confirms that the PCN maintain the original structure of $C_3N_4$.[31,32]

Figure 3 shows the morphologies of CN and PCN by scanning electron microscopy (SEM). Figure 3a, 3b show that the CN sample is thin nanosheet shape with a lateral scale of hundreds of nanometers. The representative nanosheets tends to bend and appear many flakes with some wrinkles, which is similar with the previous report.[33] After modification of PDA (Figure 3c, 3d), the PCN sample displays similar nanosheet structure like CN and no obvious aggregates were observed, which suggests that PDA self-polymerization on the CN nanosheet surface does not change its structure.[34]

X-ray photoelectron spectroscopy (XPS) was employed to investigate the chemical composition and bonding characteristics of the CN and PCN samples, as depicted in Figure 4. The XPS survey spectra revealed that both pure CN and PCN contain the same elements, namely C, N, and O (Figure 4a). However, PCN exhibits a higher percentage of C and O compared to CN, which can be attributed to the presence of PDA with a substantial amount of oxygen-containing functional groups and a reduced N content. In Figure 4b, the XPS C1s core-level spectrum of CN reveals two discrete peak constituents, characterized by binding energies of 284.6 and 288.1 eV,

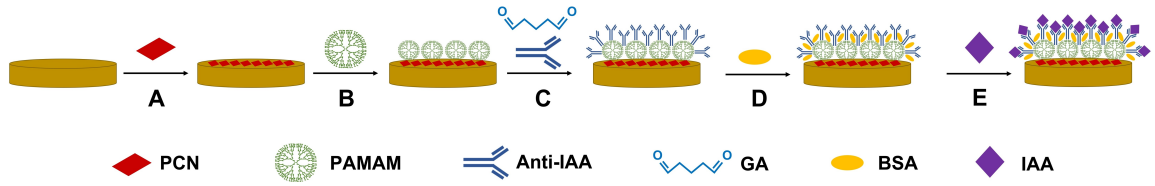


**Figure 1.** The schematic depiction outlining the preparation of the immunosensor. (A) PCN modification by drop-casting; (B) PAMAM assembly by Schiff base and Michael addition; (C) anti-IAA antibody grafting by GA crosslinking; (D) BSA blocking and (E) IAA detection.

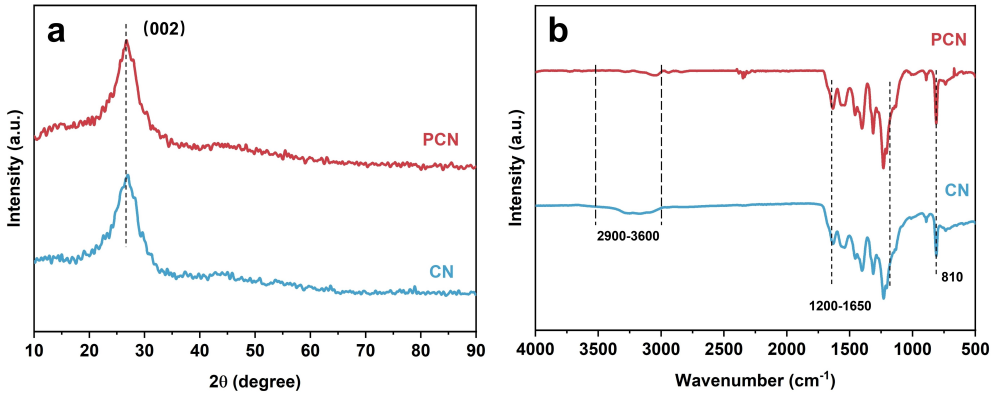


**Figure 2.** XRD patterns (a) and FTIR spectra (b) CN and PCN.

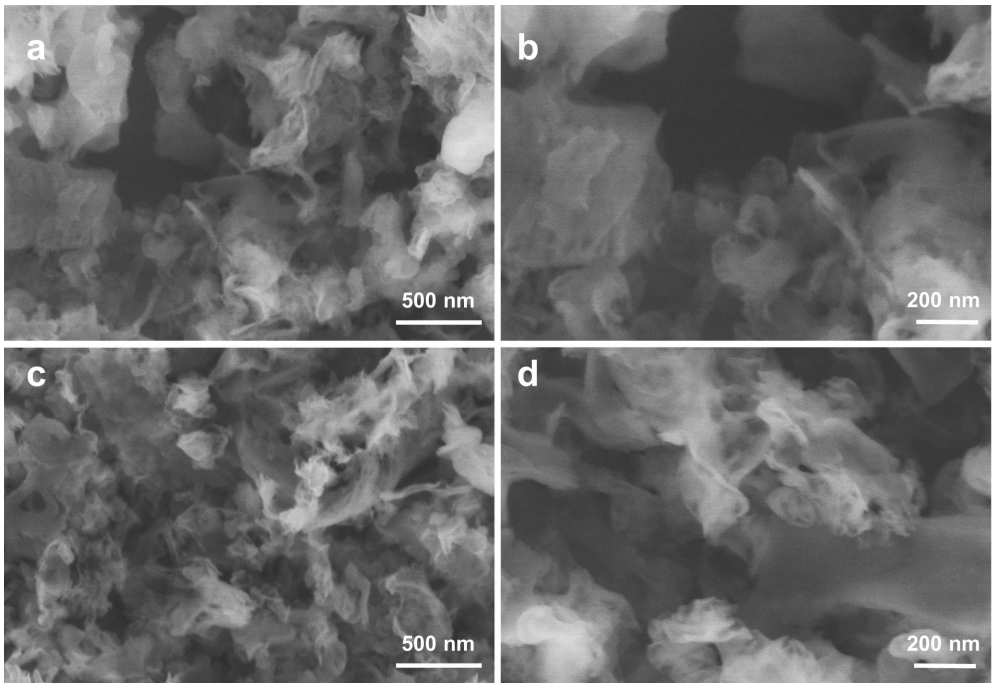


**Figure 3.** SEM images of the CN (a, b) and PCN (c, d).

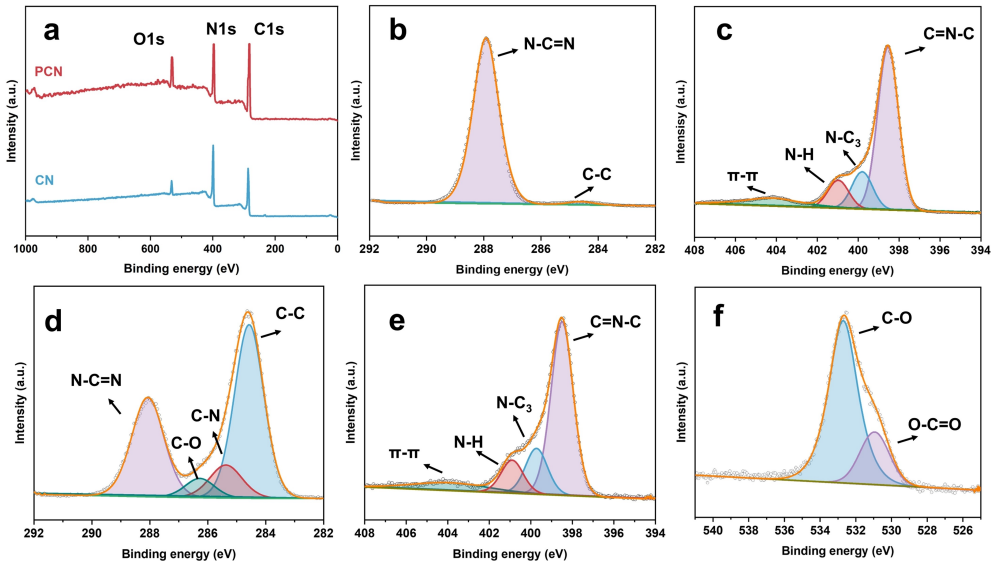


**Figure 4.** (a) XPS survey spectra of CN and PCN. High-resolution XPS spectra include (b) C1s and (c) N1s for CN, as well as (d) C1s, (e) N1s, and (f) O1s for PCN.

aligning with the C–C and N–C=N species, respectively.[30,35] In Figure 4c, the XPS N1s core-level spectrum of CN exhibits four component peaks with binding energies approximately at 398.3, 399.1, 400.6, and 404.5 eV, attributed to C=N–C, N–$C_3$, N–H bonding, and positive charge localization or charging effects, respectively.[35,36] Notably, in the C1s spectrum of PCN (Figure 4d), new peaks emerge at 285.3 and 286.2 eV, corresponding to C–N and C–O species. This is due to the presence of PDA, which has an aromatic core structure containing hydroxyl and amino groups. [30,31] In Figure 4e, the XPS N1s core-level spectrum of PCN displays similar binding energies in each corresponding peak, which is attributed to the overlapping peaks in the same region of PDA and CN.[31,37] In Figure 4f, the peaks at 531.2 and 532.7 eV appeared in PCN are assigned to O–C=O and C–O bonding, respectively.[31]

EIS emerges as a potent technique for probing the charge transfer processes occurring at the electrode interface throughout each modification step. The charge transfer resistance ($R_{ct}$) is a critical parameter signifying the hindrance encountered by charge transfer at the electrode interface.[38] As depicted in Figure 5a, the Nyquist plots for the bare Au electrode, PCN/Au, PAMAM/PCN/Au, and anti-IAA/PAMAM/PCN/Au are presented.

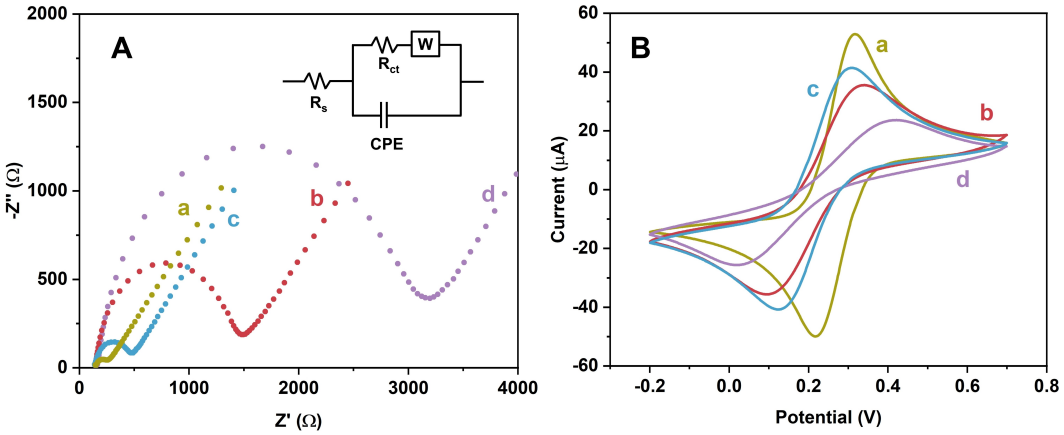


**Figure 5.** The Nyquist impedance spectra (A) and cyclic voltammograms (B) of the Au electrode, sequentially modified at various stages, immersed in the 5 mM $Fe(CN)_6^{3-/4-}$ within a 0.01 M PBS (pH 7.4) are presented. The stages include (a) Au, (b) PCN/Au, (c) PAMAM/PCN/Au, and (d) anti-IAA/PAMAM/PCN/Au.

The impedance diagrams consist of a low-frequency segment linked to diffusion control, depicted by the Warburg impedance, and a higher-frequency semicircular segment associated with the resistance of electron transfer at the electrode interface.[39,40] To analyze the impedance spectroscopy, we utilized an equivalent circuit, as illustrated in the inset of Figure 5a. The values of the equivalent circuit elements for different modified electrodes are summarized in Table S1 (Supporting Information). A smaller semicircle portion in the EIS curve corresponds to a lower charge transfer resistance ($R_{ct}$) value, beneficial for charge immigration across the electrode-electrolyte interface. It is evident that the PCN-modified Au electrode displays an enlargement of the semicircular portion (curve b) in comparison to the bare Au electrode (curve a). This increase in the $R_{ct}$ value indicates the successful assembly of PCN nanocomposites onto the electrode. It has been reported that $C_3N_4$ can tune the electrochemical impedance and electrocatalytic activity of the electrode surface.[41] The lamellar structure of $C_3N_4$ has the advantage of increasing the specific surface area and accelerating migration rate of electrons. Moreover, $C_3N_4$ is a semiconductor that can limit the transfer of electrons from the redox probe $Fe(CN)_6^{3-/4-}$ to the electrode surface.[42] In addition, the increase of $R_{ct}$ may come from the poor conductivity of PDA hindering the electron transfer at the interface.[43,44] Upon immobilizing the PAMAM layer onto the PCN-modified electrode, there is a notable reduction in the $R_{ct}$ value (curve c). This decrease can be attributed to the presence of primary amine groups on PAMAM, which readily undergo protonation. The nanoscale PAMAM molecule assumes a positively charged spherical form at a pH of 7.4. This positive charge facilitates the efficient conduction of negatively charged $Fe(CN)_6^{3-/4-}$. PAMAM, possessing a diameter of 4.5 nm, exhibits a three-dimensional structure characterized by a substantial specific surface area. This structural feature serves to significantly augment the electrode surface area, consequently enhancing the rate of electron transfer.[45,46] Nevertheless, upon the assembly of the GA layer and anti-IAA protein on the PAMAM and PCN modified electrode, the charge transfer resistance ($R_{ct}$) experiences a subsequent increase (curve d). This occurrence is attributed to the neutralization of GA molecules and the steric hindrance imposed by the anti-IAA protein. The electrode modification process was further characterized through cyclic voltammetry (CV), as depicted in Figure 5b. In comparison to the bare Au electrode (curve a), the introduction of the PCN (curve b) onto the electrode led to a decrease in peak current. Subsequent modification with the PAMAM resulted in an increased peak current (curve c), indicating enhanced electron transfer facilitated by the PAMAM. However, upon further assembly of GA and anti-IAA onto the electrode, a notable reduction in peak current occurred (curve d). Additionally, the reversibility of the redox peaks deteriorated, suggesting a hindrance to the electron transfer process. This phenomenon is likely attributed to the cumulative effect of GA and anti-IAA, acting as barriers that impede the efficient exchange of electrons, leading to reduced peak current and decreased reversibility. The results from CV were consistent with the EIS findings, confirming the successful layer-by-layer modification in the fabrication of the immunosensor.

The anti-IAA/PAMAM/PCN/Au electrode was used as a working electrode for the detection of IAA. To assess the immunosensor's reaction to IAA, it was exposed to IAA for 1 h. Subsequently, EIS measurements were conducted in the presence of the redox probe $Fe(CN)_6^{3-/4-}$. Figure 6 shows the impedimetric response of the immunosensor to different concentrations of IAA, with the $R_{ct}$ value increasing as the IAA concentration increases. This can be attributed to the formation of a complex between IAA and sensor, resulting in heightened steric hindrance.[47] Furthermore, with a pKa of 4.75, IAA carries a negative charge in PBS solution (pH 7.4), causing it to repel the negatively charged $Fe(CN)_6^{3-/4-}$, thus inhibiting electron transfer.[48]

The alteration in the charge transfer resistance ($\Delta R_{ct}$) exhibited a proportionate relationship with the logarithm of IAA concentration in the range of 10 ng/mL to 100 μg/mL, as illustrated in Figure 7 (sensor A). The correlation was expressed through the linear regression formula $\Delta R_{ct} = 402.8 \times \log c + 3554.8$ ($R^2$ 0.9994). The estimated minimum detectable concentration stood at 3.9 ng/mL (S/N = 3). In addition to the

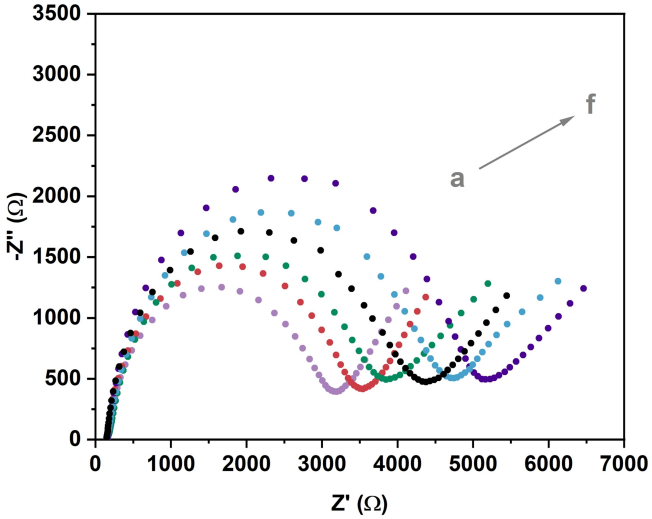


**Figure 6.** The Nyquist impedance spectra of the anti-IAA/PAMAM/PCN/Au after incubation with different concentrations of IAA (a) 0, (b) 10 ng/mL, (c) 100 ng/mL, (d) 1 μg/mL, (e) 10 μg/mL, (f) 100 μg/mL.

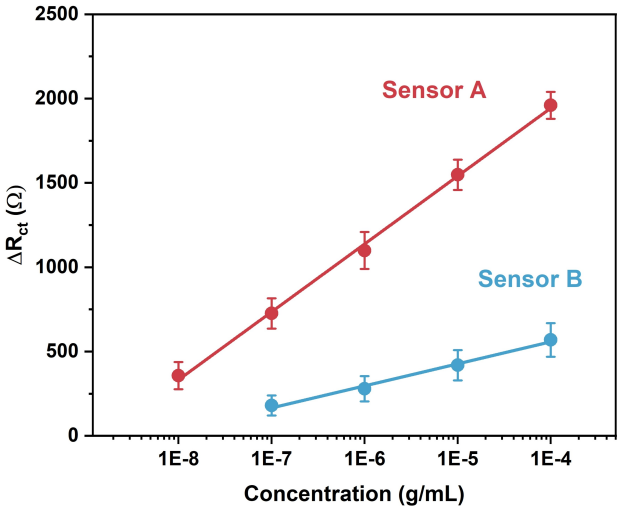


**Figure 7.** The calibration curve for two distinct immunosensors targeting IAA. The concentrations employed align with those depicted in Fig. 6. Sensor A comprises the layers anti-IAA/PAMAM/PCN/Au, while Sensor B consists of anti-IAA/PCN/Au.

developed sensor, another types of sensors without the assembly of PAMAM (anti-IAA/PCN/Au, sensor B) were prepared for comparison. Figure 7 represents the calibration curves for sensor B with the range from 100 ng/mL to 100 μg/mL. The correlation was expressed through the linear regression formula $\Delta R_{ct} = 130.7 \times \log c + 1080.6$ ($R^2$ 0.9959). The estimated minimum detectable concentration stood at 11.7 ng/mL (S/N = 3). Sensor B exhibited a notably inferior performance compared to Sensor A. This outcome underscores the synergistic effect of PAMAM and PCN in augmenting the performance of impedance immunosensors. The detection limits and linear range of this IAA electrochemical sensor is comparable to or better than some previously reported IAA sensors, as shown in Table S2 (Supporting Information).

To evaluate the selectivity of the developed immunosensor, a range of plant hormones, including succinic acid, abscisic acid, citric acid, salicylic acid, malic acid, and IAA, were employed as potential interfering substances. As showed in Figure 8, although the concentration of the interfering compounds was 100 times higher than IAA, the $\Delta R_{ct}$ values were insignificantly low, preserving the accuracy of IAA detection. These findings illustrate that the immunosensor exhibits a high level of selectivity due to the specific antibody-antigen immunoreaction. To evaluate the reproducibility, the immunosensor was subjected to five measurements of IAA at 10 ng/mL, yielding a coefficient of variation of 4.1%. Meanwhile, it was estimated by determining of IAA at 10 ng/mL with five immunosensors produced using the identical procedure, yielding a variation coefficient of 4.9%. These results collectively affirm the commendable reproducibility of the immunosensor. Moreover, following a two-week storage period at 4 °C, the immunosensor maintained 95% of its sensing capacity, highlighting its excellent stability.

The strategy of this work is to assemble PDA-modified $C_3N_4$ and PAMAM on gold electrodes to detect IAA by electrochemical impedance method, which shows great application potential in precision agriculture. However, practical applications still face some challenges. Although the detection of IAA using IAA antibodies has good specificity, it lacks universality. It is difficult to respond to other auxins naturally in plants including salicylic acid. The physiological effects of phytohormones on plant growth are the result of the synergistic effects of different phytohormones. Therefore, the trend has developed from the detection of a specific plant hormone to the simultaneous detection of multiple plant hormones. For example, electrochemical oxidation of IAA and SA under different potential windows is beneficial to their selectivity and simultaneous detection.[8,49,50] The electrochemical oxidation behavior of IAA by $C_3N_4$ is worthy of study. Another challenge is the release of plant hormones within plant tissues. In practical

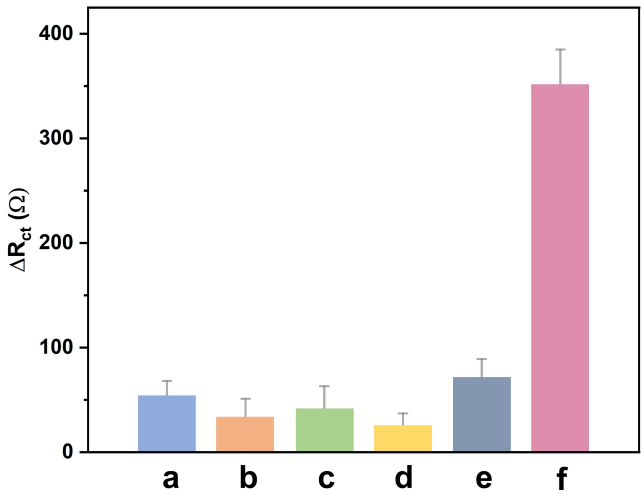


**Figure 8.** The immunosensor's EIS response to various interference species: The concentrations of a (succinic acid), b (abscisic acid), c (citric acid), d (salicylic acid) and e (malic acid) were set at 1 μg/mL, with the concentration of IAA at 10 ng/mL.

applications, the information obtained through sensors needs to reflect the overall physiological state of individual plants. The gold electrodes used in this work have large sizes, so there is an urgent need to solve the problem of how to implant electrochemical sensors into plants. Non-invasive or minimally invasive detection in vivo can be achieved using microelectrodes or microchips.[51] Modification of microelectrode surfaces for in vivo detection is the focus of future research. In addition, further research will be conducted to extend this sensor to the detection of actual samples.

## 3. Conclusions

In summary, we have developed a highly sensitive, label-free impedance immunosensor for the detection of IAA. The electrode surface was successfully modified with polydopamine-coated $C_3N_4$ nanosheets and PAMAM for subsequent immobilization of anti-IAA antibody. The layer-by-layer modification significantly enhanced the electrochemical response to trapped IAA, leading to improved detection sensitivity. The immunosensor demonstrated notable selectivity and reliable performance. The proposed method presents a promising assay platform for IAA detection, with the potential for extension to other plant hormones by substituting the anti-IAA antibody with relevant counterparts. This immunosensor holds considerable promise for applications in precision and sustainable agriculture.

## *Acknowledgements*

This research is supported by Vetenskapsrådet (2020-04096).

## *Conflict of Interests*

The authors declare no conflict of interest.

## *Data Availability Statement*

Data will be made available on request.

**Keywords:** carbon nitride · polyamidoamine · polydopamine · indole-3-acetic acid · immunosensor

[1] A. Santner, L. I. A. Calderon-Villalobos, M. Estelle, *Nat. Chem. Biol.* **2009**, *5*, 301–307.
[2] N. B. C. Serre, D. Kralík, P. Yun, Z. Slouka, S. Shabala, M. Fendrych, *Nature plants* **2021**, *7*, 1229–1238.
[3] S. Vanneste, J. Friml, *Cell* **2009**, *136*, 1005–1016.
[4] S. Cheng, J. Jiang, L. Tan, J. Deng, P. Liang, H. Su, Z. Sun, Y. Zhou, *Front. Microbiol.* **2022**, *13*, 855399.
[5] P. López-Gómez, E. N. Smith, P. Bota, A. Cornejo, M. Urra, J. Buezo, J. F. Moran, *Plants* **2022**, *11*, 1304.
[6] H. Chen, X. Guo, H. Zhang, H. Wang, *J. Chromatogr. B* **2011**, *879*, 1802–1808.
[7] D. Zhang, J. Huang, J. Hu, *Anal. Biochem.* **2022**, *649*, 114722.
[8] B. Shao, Y. Ai, L. Yan, B. Wang, Y. Huang, Q. Zou, H. Fu, X. Niu, W. Sun, *Talanta* **2023**, *253*, 124030.
[9] Y. Kuang, M. Li, S. Hu, L. Yang, Z. Liang, J. Wang, H. Jiang, X. Zhou, Z. Su, *Sensors* **2022**, *22*, 4476.
[10] H. Li, Y. Hu, A. Li, X. Wang, P. Hou, C. Wang, K. Chen, C. Zhao, *RSC advances* **2017**, *7*, 54416–54421.
[11] E. M. Rabie, A. A. Shamroukh, M. Khodari, A. Novel, *Electroanalysis* **2022**, *34*, 883–891.
[12] X. Sun, M. Duan, R. Li, Y. Meng, Q. Bai, L. Wang, M. Liu, Z. Yang, Z. Zhu, N. Sui, *Anal. Chem.* **2022**, *94*, 13598–13606.
[13] F. Polli, F. Simonetti, L. Surace, M. Agostini, G. Favero, F. Mazzei, R. Zumpano, *ChemElectroChem* **2024**, *11*, e202300408.
[14] Q. Bai, H. Luo, X. Yi, S. Shi, L. Wang, M. Liu, F. Du, Z. Yang, N. Sui, *Microchem. J.* **2022**, *179*, 107521.
[15] Z. Su, X. Xu, Y. Cheng, Y. Tan, L. Xiao, D. Tang, H. Jiang, X. Qin, H. Wang, *Nanoscale* **2019**, *11*, 962–967.
[16] Y. Hu, X. Wang, C. Wang, P. Hou, H. Dong, B. Luo, A. Li, *RSC Adv.* **2020**, *10*, 3115–3121.
[17] X. Cao, X. Zhu, S. He, X. Xu, Y. Ye, S. Gunasekaran, *Nanoscale* **2019**, *11*, 10247–10256.
[18] Z. Su, D. Tang, J. Liu, X. Yang, S. Xu, W. Xu, Y. Zhou, M. Xu, J. Yi, H. Jiang, Y. Shao, X. Qin, *J. Electroanal. Chem.* **2021**, *880*, 114855.
[19] J. B. Raval, V. N. Mehta, R. K. Singhal, H. Basu, S. Jha, S. K. Kailasa, *Trends in Environmental Analytical Chemistry* **2023**, *39*, e00205.
[20] Y. Wang, L. Liu, T. Ma, Y. Zhang, H. Huang, *Adv. Funct. Mater.* **2021**, *31*, 2102540.
[21] Y. Zheng, J. Liu, J. Liang, M. Jaroniec, S. Qiao, *Energy Environ. Sci.* **2012**, *5*, 6717–6731.
[22] Y. Wang, R. Zhang, Z. Zhang, J. Cao, T. Ma, *Adv. Mater. Interfaces* **2019**, *6*, 1901429.
[23] S. S. Low, Z. Chen, Y. Li, Y. Lu, Q. Liu, TrAC *Trends in Analytical Chemistry* **2021**, *145*, 116454.
[24] H. Lee, S. M. Dellatore, W. M. Miller, P. B. Messersmith, *Mussel-inspired surface chemistry for multifunctional coatings science* **2007**, *318*, 426–430.
[25] Y. Liu, K. Ai, L. Lu, *Chem. Rev.* **2014**, *114*, 5057–5115.
[26] J. F. Rocha, L. H. Hasimoto, M. Santiago, *Anal. Bioanal. Chem.* **2023**, *415*, 3799–3816.
[27] A. B. Asha, Y. Chen, R. Narain, *Chem. Soc. Rev.* **2021**, *50*, 11668–11683.
[28] E. B. Bahadır, M. K. Sezgintürk, *Talanta* **2016**, *148*, 427–438.
[29] M. Hasanzadeh, N. Shadjou, M. Eskandani, J. Soleymani, F. Jafari, M. de la Guardia, *TrAC Trends Anal. Chem.* **2014**, *53*, 137–149.
[30] L. Qin, D. Huang, P. Xu, G. Zeng, C. Lai, Y. Fu, H. Yi, B. Li, C. Zhang, M. Cheng, C. Zhou, X. Wen, *J. Colloid Interface Sci.* **2019**, *534*, 357–369.
[31] Z. Yu, F. Li, Q. Yang, H. Shi, Q. Chen, M. Xu, *ACS Sustainable Chem. Eng.* **2017**, *5*, 7840–7850.
[32] F. He, G. Chen, Y. Yu, Y. Zhou, Y. Zheng, S. Hao, *Chem. Commun.* **2015**, *51*, 6824–6827.
[33] P. Niu, L. Zhang, G. Liu, H. Cheng, *Adv. Funct. Mater.* **2012**, *22*, 4763–4770.
[34] X. Zhang, J. Yu, W. Macyk, S. Wageh, A. A. Al-Ghamdi, L. Wang, *Adv. Sustainable Syst.* **2023**, *7*, 2200113.
[35] M. R. Gholipour, F. Béland, T. O. Do, *ACS Sustainable Chem. Eng.* **2017**, *5* 213–220.
[36] J. Cai, J. Huang, S. Wang, J. Iocozzia, Z. Sun, J. Sun, Y. Yang, Y. Lai, Z. Lin, *Adv. Mater.* **2019**, *31*, 1806314.
[37] Z. Gong, L. Chen, K. Chen, S. Gou, X. Zhao, L. Song, J. Ma, L. Han, *J. Environ. Chem. Eng.* **2023**, *11*, 109405.
[38] J. Muñoz, R. Montes, M. Baeza, *TrAC Trends Anal. Chem.* **2017**, *97*, 201–215.
[39] J. S. Daniels, N. Pourmand, *Electroanalysis* **2007**, *19*, 1239–1257.
[40] J. F. Rubinson, Y. P. Kayinamura, *Chem. Soc. Rev.* **2009**, *38*, 3339–3347.
[41] W. Wang, J. Zhao, Y. Sun, H. Zhang, *RSC Adv.* **2019**, *9*, 7737–7746.
[42] X. Liu, J. Zhang, J. Di, Y. Long, W. Li, Y. Tu, *J. Colloid Interface Sci.* **2017**, *505*, 964–972.
[43] J. Sun, G. Wang, H. Cheng, Y. Han, Q. Li, C. Jiang, *Bioelectrochemistry* **2022**, *145*, 108073.
[44] G. Wang, Q. Xu, L. Liu, X. Su, J. Lin, G. Xu, X. Luo, *ACS Appl. Mater. Interfaces* **2017**, *9*, 31153–31160.
[45] G. Li, X. Li, J. Wan, S. Zhang, *Biosens. Bioelectron.* **2009**, *24*, 3281–3287.
[46] J. Xu, X. Wang, C. Yan, W. Chen, *Sensors* **2019**, *19*, 1879.

[47] H. Yin, Z. Xu, Y. Zhou, M. Wang, S. Ai, *Analyst* **2013**, *138*, 1851–1857.
[48] Z. Chen, Z. Lin, L. Zhang, Y. Cai, L. Zhang, *Analyst* **2012**, *137*, 1723–1729.
[49] H. Li, C. Wang, X. Wang, P. Hou, B. Luo, P. Song, D. Pan, A. Li, L. Chen, *Biosens. Bioelectron.* **2019**, *126*, 193–199.
[50] L. Tang, D. Li, W. Liu, Y. Sun, Y. Dai, W. Cui, X. Geng, D. Li, F. Song, L. Sun, *Biosensors* **2023**, *13*, 1002.
[51] Z. Li, J. Zhou, T. Dong, Y. Xu, Y. Shang, *Biosens. Bioelectron.* **2021**, *182*, 113105.

Manuscript received: February 12, 2024
Revised manuscript received: March 13, 2024
Version of record online: ■■, ■■

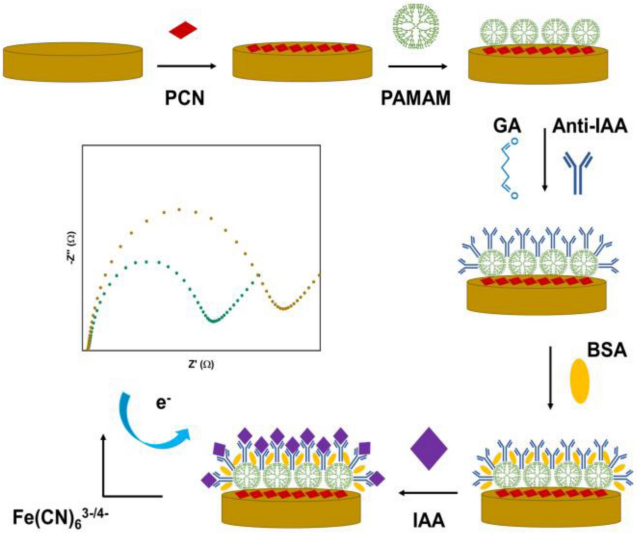


*J. Zhang, A. Li, X. Yu, I. Mijakovic, S. Pandit**

1 – 9

**Polydopamine Modified Carbon Nitride and PAMAM Assembled Electrochemical Immunosensor for Detection of Indole-3-Acetic Acid**

An electrochemical immunosensor was developed for precise detection of indole-3-acetic acid (IAA), a crucial plant phytohormone. Utilizing polydopamine modified $C_3N_4$ nanosheets (PCN) and polyamidoamine dendrimer (PAMAM), the sensor enhanced antibody immobilization, improving IAA capture and electrochemical response. The method offers high sensitivity, selectivity, and potential for broader phytohormone detection, presenting an alternative to IAA-based detection.